Earth and Space Science

RESEARCH ARTICLE
10.1029/2020EA001529

A Synoptic-Scale Wavelike Structure in the Nighttime Equatorial Ionization Anomaly

J. Rodríguez-Zuluaga[1], C. Stolle[1,2], Y. Yamazaki[1], C. Xiong[1], and S. L. England[3]

[1]GFZ German Research Centre for Geosciences, Potsdam, Germany, [2]Faculty of Science, University of Potsdam, Potsdam, Germany, [3]Aerospace and Ocean Engineering, Virginia Polytechnic Institute and State University, Blacksburg, VA, USA

Key Points:

- Characteristics of a wavelike structure in the nighttime equatorial ionization anomaly are reported using GOLD far-ultraviolet observations
- The structure is symmetric about the dip equator, appears stationary with time over the night, and is highly variable on a day-to-day basis
- A cluster or quasi-periodic wave train of equatorial plasma depletions is often detected within the synoptic structure

Correspondence to:
J. Rodríguez-Zuluaga,
juanrz@gfz-potsdam.de

Citation:
Rodríguez-Zuluaga, J., Stolle, C., Yamazaki, Y., Xiong, C., & England, S. L. (2021). A synoptic-scale wavelike structure in the nighttime equatorial ionization anomaly. *Earth and Space Science*, *8*, e2020EA001529. https://doi.org/10.1029/2020EA001529

Received 22 OCT 2020
Accepted 27 DEC 2020

Abstract Both ground- and satellite-based airglow imaging have significantly contributed to understanding the low-latitude ionosphere, especially the morphology and dynamics of the equatorial ionization anomaly (EIA). The NASA Global-scale Observations of the Limb and Disk (GOLD) mission focuses on far-ultraviolet airglow images from a geostationary orbit at 47.5°W. This region is of particular interest at low magnetic latitudes because of the high magnetic declination (i.e., about -20°) and proximity of the South Atlantic magnetic anomaly. In this study, we characterize an exciting feature of the nighttime EIA using GOLD observations from October 5, 2018 to June 30, 2020. It consists of a wavelike structure of a few thousand kilometers seen as poleward and equatorward displacements of the EIA-crests. Initial analyses show that the synoptic-scale structure is symmetric about the dip equator and appears nearly stationary with time over the night. In quasi-dipole coordinates, maxima poleward displacements of the EIA-crests are seen at about ± 12° latitude and around 20 and 60° longitude (i.e., in geographic longitude at the dip equator, about 53°W and 14°W). The wavelike structure presents typical zonal wavelengths of about 6.7×10^3 km and 3.3×10^3 km. The structure's occurrence and wavelength are highly variable on a day-to-day basis with no apparent dependence on geomagnetic activity. In addition, a cluster or quasi-periodic wave train of equatorial plasma depletions (EPDs) is often detected within the synoptic-scale structure. We further outline the difference in observing these EPDs from FUV images and in situ measurements during a GOLD and Swarm mission conjunction.

1. Introduction

The Earth's ionosphere is the layer of the upper atmosphere ionized via extreme ultraviolet solar radiation and particle precipitation. At mid and low magnetic latitudes, the former mechanism is the primary source of plasma. The region with the highest plasma density is typically found at about 300–400 km altitude, consisting mainly of atomic oxygen ions (O^+). It is referred to as F-region and is generally treated as a collisionless environment. However, collisions with neutrals are essential when referring to coupling with the lower thermosphere (e.g., Liu et al., 2009). In the E-region, between 100 and 150 km, collisions happen much more frequently, resulting in faster recombination and a significant reduction of the plasma density right after sunset (Heelis, 2004).

At low magnetic latitudes, the ionosphere presents a bimodal meridional distribution of the plasma centered at the dip equator. This regular structure is commonly referred to as the equatorial ionization anomaly (EIA) (Appleton, 1946). The EIA is formed due to the uplift of plasma at the dip equator by eastward dynamo electric fields in the E- and F-regions and its subsequent downward diffusion along magnetic field lines (Duncan, 1960). Variations in any of these processes, especially in the dynamo-electric field, can cause substantial changes in the EIA morphology. By using far-ultraviolet (FUV) emissions measured by the IMAGE satellite mission, Immel et al. (2006) reported a repeated separation and rapprochement of the EIA-crests seen as a wavenumber four structure. The authors analyzed the correspondence between the tidal temperatures in the E-region and both the latitude and brightness of the EIA-crests. With an excellent match among these parameters, the authors showed the effect of atmospheric tides on the EIA morphology. Recently, using FUV images from the Special Sensor Ultraviolet Spectrographic Imager (SSUSI) instrument onboard the Defense Meteorological Satellite Program (DMSP) F18, Guo et al. (2020) have identified evidence of wavenumbers 1 to 4 in the EIA and reported significant annual and semiannual periods of these wave structures.

An interesting phenomenon of the nighttime EIA is the existence of plasma instabilities. After sunset at the dip equator, the sharp vertically upward gradient of the plasma density, the magnetic field, and currents driven by the background electric field and gravity are mutually perpendicular. This configuration allows interchange instabilities to operate and generate plasma irregularities; commonly called equatorial spread F (Hysell, 2000). The structures of the spread F within 10s–100s of kilometers, generally known as equatorial plasma depletions (EPDs), can reach altitudes of up to 2,000 km. Since they are mapped along the magnetic field lines, they can disrupt the post-sunset EIA's ionospheric density profile. This phenomenon is observed as wedge-like density depleted channels in global observations (e.g., Eastes et al., 2019; Kil et al., 2009).

A well-established feature of the low latitude ionosphere is a brief and intense lifting of the F-region produced by an increase of the dayside eastward electric field, just before its nighttime reversal (e.g., Kelley et al., 2009; Richmond et al., 2015). This phenomenon, named pre-reversal enhancement (PRE), causes an intensified vertical uplift of the ionosphere, favoring the generation of EPDs (e.g., Basu et al., 1996). The agreement between the longitudinal and seasonal variability of both the PRE and EPDs occurrence has been already shown (e.g., Huang & Hairston, 2015; Stolle et al., 2008). Even though this is evident in the climatological sense, the day-to-day variability of the vertical drift does not seem to agree with that of the occurrence of EPDs (e.g., Hysell & Burcham, 2002). Since EPDs tend to occur in clusters or quasi-periodic wave trains (e.g., Eastes et al., 2019; Makela et al., 2010), it has been suggested they might result from the electrodynamical process within an upwelling, generally amplified by the post-sunset rise of the F-region due to the PRE (Tsunoda et al., 2018). Different phenomena such as gravity waves (Singh et al., 1997) and shear flow (Hysell & Kudeki, 2004) seem capable of forming localized upwellings that can explain these observations.

In this study, we use FUV images of the nighttime ionosphere by the Global-scale Observations of the Limb and Disk (GOLD) mission to investigate a synoptic-scale wavelike structure in the EIA-crests observed between about 80°W and 10°E longitude. This phenomenon is seen as poleward and equatorward displacements of the EIA-crests in a short longitude distance. It is symmetric about the dip equator and nearly stationary with time over the night. Within these structures, there are clusters of EPDs shaped in latitude by the EIA-crests. This work aims to report characteristics of this phenomenon, such as location, zonal wavelength, amplitude, day-to-day variability and potential relation to the occurrence of EPDs.

2. GOLD Far-Ultraviolet Nightglow Observations

At night, emissions from the ionosphere come from radiative processes in the F-region either by recombination of atomic oxygen ions with electrons ($O^+ + e$) or ion-ion mutual neutralization ($O^+ + O^-$). Both processes generate an excited state of atomic oxygen (O I). The brightness of these emissions is directly proportional to the plasma density squared (Kelley et al., 2003). It means that a significant plasma density is required to emit a detectable quantity. Because the number of oxygen ions and electrons varies considerably with altitude, the emissions are assumed primarily from the F peak - the region where their densities are the highest and nearly alike. Since the recombination rates are sufficiently slow in the F-region, areas of enhanced ion density such as the EIA's crests may persist through the night. The most significant emission of the EIA observed at night is O I 135.6 nm. GOLD is a NASA mission launched on January 25, 2018. It observes the far-ultraviolet (FUV) spectrum of Earth's atmosphere (ca. 134–162 nm). The instrument is a dual-channel (A and B), spectral imager hosted in geostationary orbit on SES-14, a satellite located at 47.5°W longitude (Eastes et al., 2020). Nighttime scans cover about 45° of longitude, maintaining a cadence of 15 min per scan. From 20:10 to 23:10 UT, channel-B scans alternate between both hemispheres. From 23:10 to 00:40 UT, channel-A scans the northern hemisphere while channel-B scans the southern hemisphere. Figure 1 displays a sequence of GOLD FUV images showing both the nighttime EIA-crests and EPDs, seen as black stripes perpendicular to the dip equator (solid yellow line). An exciting observation is a substantial change of the EIA morphology over a short longitude distance - far less than the well-known wavenumber 4 (zonal wavelength of 90°, circa 1.0×10^4 km). It consists of displacements of the EIA-crests away from and toward the dip equator, seen as a synoptic-scale wavelike structure. For this particular night, the EIA-struc-

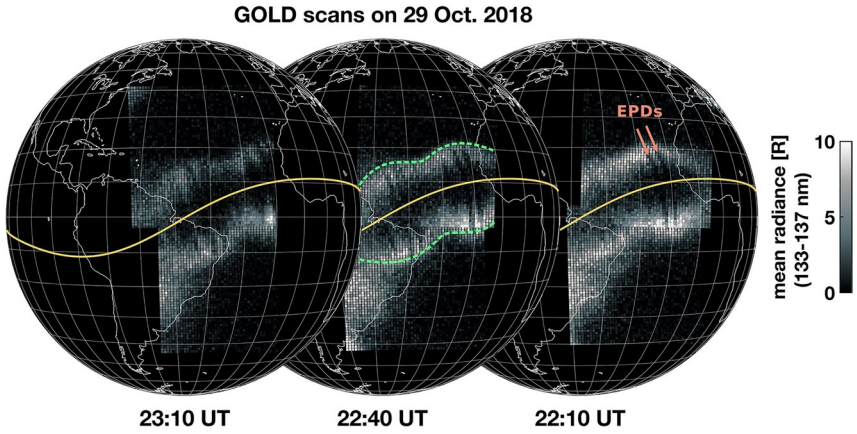

Figure 1. Example of three consecutive images of GOLD on October 29, 2018. It depicts a synoptic-scale wavelike feature in the EIA-crests highlighted by green dashed-lines and equatorial plasma depletions (EPDs) seen as black stripes and indicated by red arrows. Each image displays two scans. The time at the bottom of each image corresponds to the starting time of the northern scan. Each scan takes about 15 min. The dip equator is displayed as a yellow line.

ture presents two nearly symmetric poleward displacements, both with EPDs whose latitudinal extension follows the EIA-crests.

3. Synoptic-Scale Wavelike Structure in the EIA

To describe EIA's morphology, we use GOLD nighttime scans (NI1) from October 5, 2018 to June 30, 2020. Because of the high magnetic declination in the region covered by the GOLD scans (c.a., -20°), and the conjugate character between magnetic hemispheres of both the wavelike structures and EPDs, we use quasi-dipole coordinates throughout the study. The processing starts by converting each FUV image (single scan) from geographic to quasi-dipole coordinates. To obtain a single FUV image of both hemispheres (sFUVI), like the one in Figure 2a, consecutive or simultaneous scans of the two hemispheres are set to a $1 \times 1°$ grid of quasi-dipole longitude and latitude. Each sFUVI only comprises longitudes common to both scans. In areas where the two scans overlap, the northern scan is considered. As mentioned earlier, channel-B scans alternating between both hemispheres from 20:10 to 23:10 UT. In this interval, an sFUVI comprises two scans shifted by 15 min. From 23:10 to 00:40 UT, sFUVIs are based on simultaneous scans of the northern and southern hemispheres by channel-A and channel-B, respectively.

A single day generally comprises 13 sFUVI. As a requisite, we only consider days with complete and successive sFUVIs at least between 21:10 and 23:55 UT. Since the structure appears nearly stationary with time,

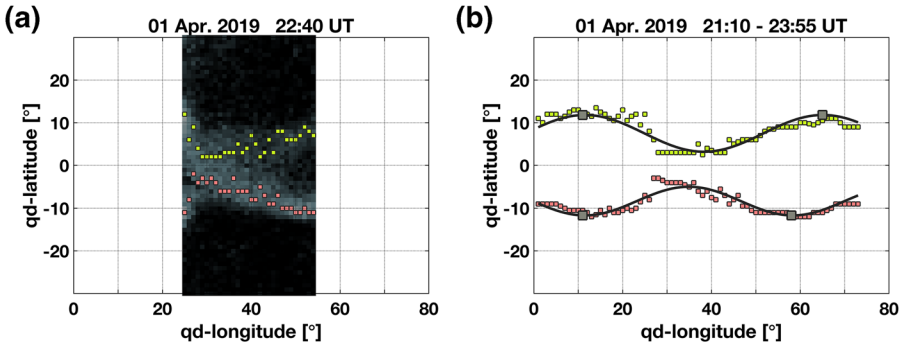

Figure 2. (a) Single FUV image of both hemispheres (sFUVI). Green and pink squares indicate the detection of the EIA-crests. The time on the title indicates the start of the scans. (b) Position of the EIA-crests from all the sFUVI on April 1, 2019. The time of the beginning of the first and last scan is indicated. Thick black lines are nonlinear regressions fitting the green and pink squares. Gray squares indicate the maxima latitudinal values.

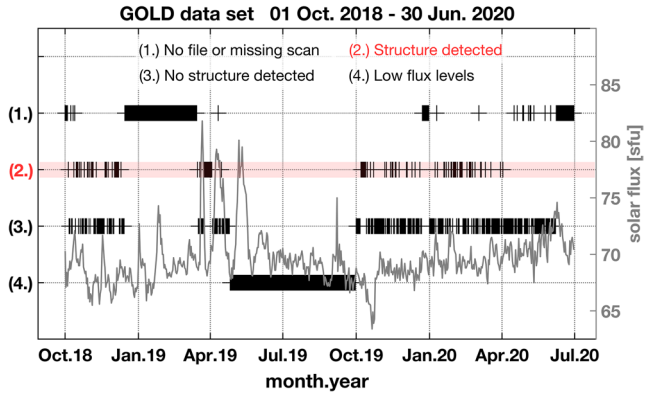

Figure 3. GOLD data set description and solar flux for the period between October 1, 2018 and June 30, 2020. Highlighted in red are the data used in this study. The solar radio flux at 10.7 cm (F10.7 index) is provided as a reference.

we can use successive sFUVIs without a jump at the boundaries between sFUVIs. To characterize the synoptic-scale structure, we detect the EIA-crests in all sFUVIs. For every degree of longitude, we select the pixel with the highest value at each magnetic hemisphere (green and pink squares in Figure 2a). After that, we merge the output from all the daily sFUVIs, remove outliers using a 5° window in longitude, and get a median value per degree of longitude (green and pink squares in Figure 2b). Finally, we use nonlinear regression to find the sinusoidal function that best fits each EIA-crest morphology, independently (solid black line in Figure 2b). The zonal wavelengths and amplitudes we use in this study correspond to those of the sinusoidal fitting curve.

Finally, 95 wavelike structures are selected (one per day). The selection corresponds to structures with zonal wavelengths between 20 and 100°, and amplitudes at both EIA-crests greater than or equal to 1°. Wavelengths greater than 100° did not present a well-defined wavelike structure in the FUV images. Wavelengths of less than 20° were mostly related to issues in the EIA-crests' detection associated with noisy FUV images or cases with no clear EIA structure. Furthermore, there are gaps in the data set either due to missing scans or images with very low flux levels (blank images). Figure 3 displays a description of the data set. It indicates when: (1) there were no files, or missing scans, (2) a wavelike structure was detected and used in this study, (3) the structure recognized did not comply with the requirements above, and (4) the FUV image was blank due to low flux levels.

Interestingly, the synoptic-scale wavelike structure is not local time-dependent, which means it is observed as steady-structures centered at specific longitudes throughout the night. This feature is already evident in the example shown in Figure 2b, which, as explained above, it is the result of combining consecutive daily sFUVIs. It is also observed that their morphology varies from day-to-day. Figure 4 displays four typical structures found in the GOLD FUV images. The plots describe, (a) a no wavelike structure,

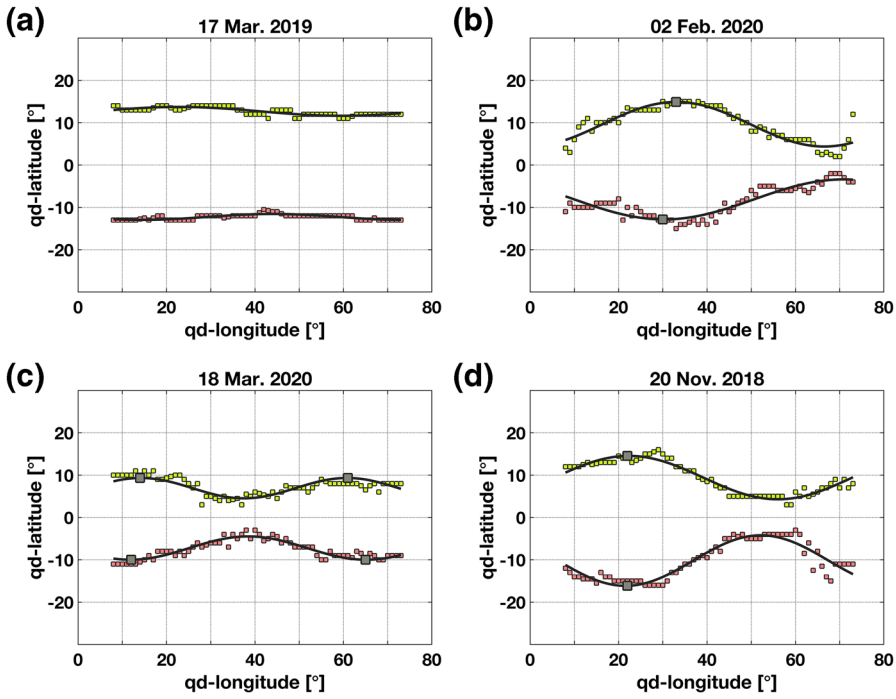

Figure 4. Typical observations of the EIA in GOLD FUV images. (a) No wavelike structure. (b) Single structure. (c) Double structure. (d) Apparent double structure with one part out of the range (more than half). Gray squares indicate the maxima latitudinal displacements.

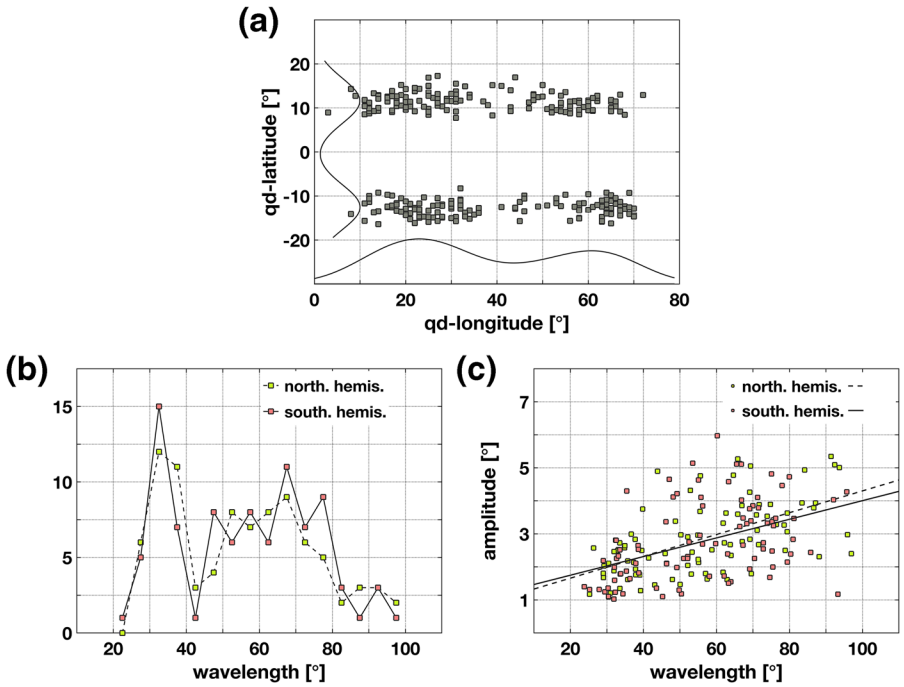

Figure 5. (a) Spatial distribution of the maximum latitudinal displacement of each wavelike structure event. Solid black lines represent their density distribution. (b) The number of events as a function of zonal wavelength for the northern and southern magnetic hemispheres. (c) Variation of the amplitude as a function of zonal wavelength for the northern and southern EIA-crests separately. Correlation coefficients of 0.58 and 0.45, respectively.

(b) a single structure, (c) a double structure, and (d) an apparent double structure with one part out of the range (more than half). The latter case is considered as a single structure. From all the structures found in this study (95 cases), 60.87% are single, and 39.13% are double. It is important to note that these four examples do not constitute any classification of the phenomenon. They merely show how the EIA-structure lines up with GOLD's FUV.

To assess the location of the synoptic-scale structure, we detect the position of the maximum latitudinal displacement of the EIA-crests (i.e., gray squares in Figures 2b and 4). They are generally located at about 20 and 60° of quasi-dipole longitude (i.e., in geographic longitude about 53°W and 14°W at the dip equator), and ± 12° of quasi-dipole latitude, as seen in Figure 5a. Regarding their associated zonal wavelength, Figure 5b shows a general preference for values around 35 and 65° (i.e., ca. 3.3×10^3 km and 6.7×10^3 km, respectively). However, values around the maximum at 65° suggest a higher variability, with a range of wavelengths expanding from about 45° to 80°. Another observation is the apparent correlation between the amplitudes and zonal wavelengths of the EIA-structure. Figure 5c depicts the relation between these two parameters separately for the northern and southern EIA-crests. The correlation coefficients are 0.58 and 0.45, respectively. Even though they do not represent a high correlation, there seems to be an interesting tendency for the EIA-structure to simultaneously expand in both latitude and longitude.

It is important to mention that variations from one day to another of the structures' wavelength do not show any apparent periodicity or dependence on geomagnetic activity. Figure 6a shows for a sample period, variations of the zonal wavelength of the northern EIA-crest on a day-to-day basis. Even though the events are not equally spaced in time, it is easy to note the high variability of the zonal wavelength from one day to another. Figure 6bdepicts variations of the northern EIA-crest wavelengths for the 95 cases as a function of geomagnetic activity (3-h Kp index). Since a single event is composed of complete and consecutive sFUVIs at least between 21:10 and 23:55 UT, we have selected the Kp index for the last 3 h of the corresponding day (i.e., 21–24 UT). With a correlation coefficient of -0.02, we conclude that this phenomenon does not depend on geomagnetic activity.

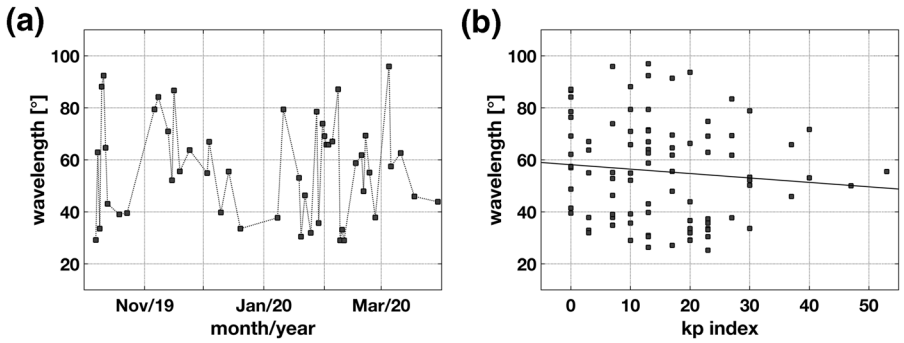

Figure 6. (a) Day-to-day variations of the northern EIA-crest wavelength for a sample period. (b) Variations of the northern EIA-crest wavelength as a function of geomagnetic activity, as denoted by the Kp index (R = -0.02).

4. Discussion

Based on the results above, we can highlight three main characteristics of the nighttime EIA's synoptic-scale structure. It is symmetric about the dip equator, remains nearly stationary with time over the night, and presents a high variability on a day-to-day basis with no dependence on geomagnetic activity. The symmetric poleward and equatorward displacements of the EIA-crests suggest that the underlying mechanisms perturb the vertical plasma drift (i.e., the EIA's fountain effect). Regarding the EIA morphology, studies have shown how atmospheric tides can modify the daytime eastward dynamo electric field at low magnetic latitudes; therefore, the vertical plasma drift. England et al. (2006) used a set of observations from IMAGE FUV, TIMED GUVI, and OGO D 12 to show that the well-known EIA wavenumber four structure is the results of non-migrating diurnal tides at E region altitudes. They demonstrated that the good correlation between the tidally modulated winds and temperatures in the lower thermosphere could explain the EIA's fountain effect's modulation. Further studies have also shown climatological analysis of wavelike structures in the EIA. A recent study by Guo et al. (2020) shows global nighttime airglow images from the SSUSI instrument onboard the DMSP F18. The authors reported evidence of wavenumbers one to 4 with different annual and semiannual periods among them. The reason why some earlier studies have not detected synoptic-scale structures is because of their substantial phase variability. As demonstrated in this paper, the wavelike structure phase presents large changes on a day-to-day basis (see Figure 6a). In climatological studies, the data that contain wavelike structures with different phases are analyzed together. Climatological averaging would remove a large part of wave structures even if they existed in the data. It is interesting, however, to find in the results of England et al. (2006), two synoptic-scale structures at about 50°W and 30°W longitude between two peaks of the global wavenumber four feature. Even though we cannot prove they are the structures we address in this study, they should be considered in further analysis.

Figure 5b shows typical zonal wavelengths of about 35 and 65°, with the latter value having a more significant spread. These two values are associated with single structures of half of their wavelengths, like the ones in Figures 4c and 4b, respectively. By taking into account that the PRE's typical duration is 2 h (Fejer et al., 1991), its associated uplift generally extends over 30° in longitude. Commonly, models and observations have presented large-scale and smooth longitudinal variations of the PRE. If so, this mechanism could not explain structures like the ones reported in this study due to its continuous and long-lasting effect across much longer zonal distances. Nevertheless, using the Whole Atmosphere Community Climate Model with thermosphere and ionosphere extension (WACCM-X), Liu et al. (2018) showed that the PRE presents a substantial day-to-day variability. Figure 11 in the study by Liu et al. (2018) presents daily values of PRE under high and low solar flux conditions. Interesting is the longitudinal variation of a few tens of degrees observed between days. Significant sharp longitudinal gradients of this kind have also been observed in the daytime zonal electric field and total electron content (e.g., Alken et al., 2015; Anderson et al., 2009). Although these results cannot be directly compared with ours because of the different methodologies, these gradients represent a scale of dynamics whose characterization and identification of sources are essential in studying synoptic-scale structures.

The strong day-to-day variability of both the occurrence of the EIA-structure and its associated zonal wavelength and the non-dependence on geomagnetic activity (see Figure 6) suggest the driving mechanism being of a highly variable nature. To unveil the phenomenon responsible for the local modulation of the nighttime EIA, we need further studies. Two possible candidates might be the superposition of two or more tides or large-scale gravity waves. In the first case, the change of amplitudes/phases of tides could result in smaller wavelike structures with high day-to-day variability. Different studies have addressed tidal variability in the ionosphere (e.g., Forbes et al., 2008). They usually do not focus on tides with zonal wave numbers larger than six, as those tidal components are less significant in global climatology. In this regard, we need dedicated studies to evaluate how powerful tides with large wavenumbers could be on a daily basis. Concerning gravity ways (GWs), it is known that small- and medium-scale GWs dissipate momentum in the thermosphere. This localized momentum deposition can create horizontal thermospheric body forces with large sizes and amplitudes and generate large-scale secondary GWs. Evidence has been reported by Vadas and Liu (2009) using numerical models. The authors studied the thermosphere and ionosphere's response to the dissipation of small- and medium-scale GWs excited by a deep convective plume in Brazil. They found that secondary GWs with zonal wavelengths of about 2000 km are generated. GWs with wavelengths greater than 2,000 km have earlier been detected by satellites (e.g., Bruinsma & Forbes, 2008; Forbes et al., 1995; Mayr et al., 1990). When it comes to the synoptic-scale wavelike structure observed in GOLD FUV, which appears stationary through the night, one might assume that the driving wave does not need to be stationary for many hours. If there is transient forcing to lift the ionosphere (e.g., a large-scale GW), the resulting EIA wavelike feature will remain for hours due to slow recombination—especially the radiative recombination of atomic oxygen ions (Hanson, 1969). The GOLD observations are locally near the Andes mountain range, known to be a source of GWs, especially to the west, over Argentina (e.g., Spiga et al., 2008). Other nearby regions believed to be sources of GWs are the Amazon rainforest and the Antarctic Peninsula. Even though there are different GWs hotspots such as in the central/west of the United States and Canada, central Africa, north and central Europe, and South Asia, the ones in the American sector are the most extensive (Hoffmann et al., 2013).

Independent of the mechanisms responsible for the modulation of the nighttime EIA, the variation of the plasma uplift in the nighttime EIA directly affects the occurrence of EPDs. As shown in Figure 1, the latitudinal extension of the EPDs follows the EIA-crests. At the center of the structures (i.e., where the EIA-crests reach their maximum latitude), EPDs exhibit the most significant latitudinal extension, suggesting a larger growth rate than their neighboring EPDs, therefore, a larger vertical drift. It is also noticed in the FUV images that EPDs generally appear in the EIA-crests, but no structure is seen near the dip equator. As previously mentioned, airglow emissions require a significant quantity of plasma density to be measured. Kelley et al. (2003) describe the brightness of these emissions to be approximately equal to the line integral of the electron density squared times a recombination coefficient. That said, fine structures such as those of EPDs are much easier to sort out by FUV images in the EIA-crest than between them, where the plasma density is relatively low, especially during nighttime. In contrast, in situ satellite-observations show clear structures of EPDs at the dip equator. Figure 7 presents simultaneous observations of a set of EPDs by the Swarm and GOLD missions. Swarm is an ESA constellation satellite mission widely used in studying ionospheric phenomena (e.g., Chartier et al., 2018; Park et al., 2020; Rodríguez-Zuluaga et al., 2019; Xiong et al., 2016). In the right panel, a train of EPDs is seen in the FUV image, of which three (numbered and indicated by white arrows) are intercepted by both Swarm Alpha and Charlie satellites (pink lines). From the FUV images, the separation between the three EPDs is not evident at the dip equator; however, in situ plasma density measurements displayed on the left side clearly show strong depletions near and at the dip equator. Among the 95 wavelike events considered, 83 cases (87.4%) present well-defined EPDs. Nevertheless, based on the previous observations by Swarm and GOLD, small EPDs confined to latitudes closed to the dip equator are likely not to be detected by FUV images.

Climatologically, the occurrence of EPDs has been associated with the sudden post-sunset rise of the ionosphere due to the PRE (e.g., Fejer et al., 1999; Gentile et al., 2006; Stolle et al., 2008; Su et al., 2008). Nevertheless, the presence of EPDs as clusters or quasi-periodic wave train (e.g., Eastes et al., 2019; Makela et al., 2010) cannot be explained by the local time (longitudinal) variability of the PRE. On the other side, different phenomena such as gravity waves (Singh et al., 1997) and shear flow (Hysell & Kudeki, 2004) seem capable of forming localized upwellings to explain these observations. Another relevant phenomenon to

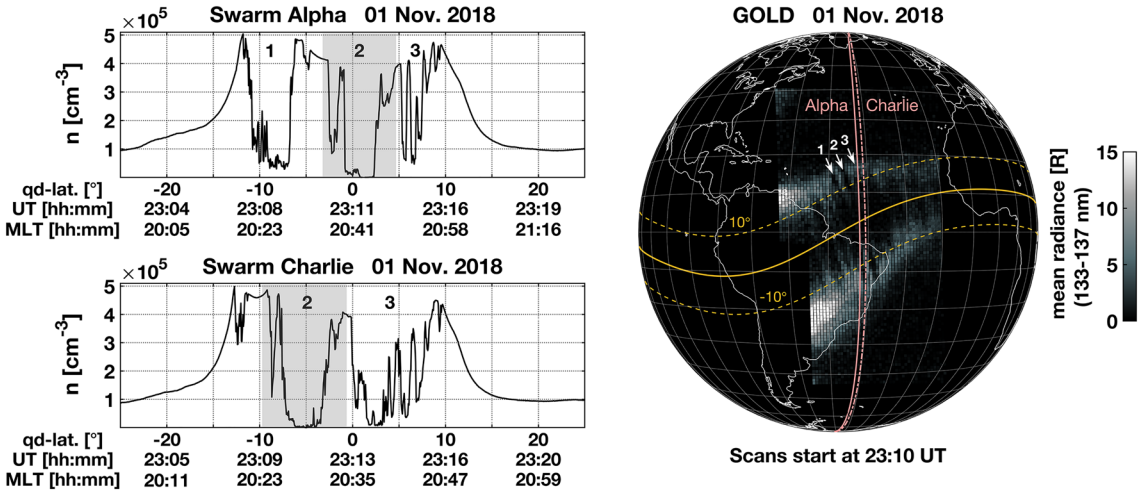

Figure 7. Simultaneous observations of GOLD and Swarm on November 1, 2018. On the right, GOLD FUV scans start at 23:10 UT. The dip equator and ±10° of quasi-dipole latitude are shown as solid and dashed yellow lines. Pink lines show Swarm Alpha and Charlie's orbits intercepting equatorial plasma depletions (EPDs) noted with white numbers and arrows. On the left, two panels present in situ measurements of the plasma density as a function of quasi-dipole latitude, universal time, and magnetic local time. They correspond to the orbits shown on the right plot. EPDs are numbered to match those in the FUV image.

understand the development of EPDs is the large-scale wave structure (LSWS). This density oscillation arises at the bottomside F-region around the PRE time with zonal wavelengths ranging from 300 km to 800 km (e.g., Thampi et al., 2009; Tsunoda et al., 2011). The relationship among these phenomena is still unknown, and the apparent effect of the EIA's synoptic structure on EPDs brings up the need for further studies. It also highlights the importance of understanding the EIA modulations' nature at synoptic- and meso-scales.

5. Summary and Conclusions

We report the characterization of a synoptic-scale wavelike structure observed in the nighttime equatorial ionization anomaly, EIA. The structure is seen as poleward and equatorward displacements of the EIA-crests over a short longitude distance. We use GOLD FUV images from October 5, 2018 to June 30, 2020 to assess spatial and temporal characteristics. A few events are currently available such that only a limited statistical analysis can be performed. The main findings are as follows:

1. The synoptic-scale structure is symmetric about the dip equator. This suggests the underlying mechanisms is perturbing the vertical plasma drift (i.e., EIA's fountain effect)
2. It appears stationary with time over the night. In quasi-dipole coordinates, the maxima poleward displacements of the EIA-crests are located at about ±12° latitude and 20 and 60° longitude (i.e., in geographic longitude about 53°W and 14°W at the dip equator)
3. The typical zonal wavelengths are about 35 and 65° (i.e., about 3.3×10^3 km and 6.7×10^3 km, respectively)
4. There is a strong day-to-day variability of their occurrence and zonal wavelength, with no dependence on geomagnetic activity
5. EPDs are seen to be modulated by the synoptic-scale structure. Among the 95 cases considered in this study, 83 (87.4%) present well-defined EPDs. Within the wavelike structure, the latitudinal extension of the EPDs coincides with the EIA-crests
6. A conjunction event between GOLD FUV images and Swarm orbits show that EPDs detected with GOLD are also significantly structured equatorward of the EIA-crests, although the low flux levels of FUV images cannot resolve it

Due to the high day-to-day variability of the synoptic-scale structure (i.e., occurrence and zonal wavelength), we suspect that variable wave forcing from the lower part of the atmosphere might be the source of the modulation of the fountain effect. The observed short zonal wavelength could result from large-scale gravity waves or the superposition of two or more tidal waves. In addition, the agreement between the

latitudinal displacement of EPDs and the EIA-crests suggests an effect of the synoptic-scale structure on the occurrence of EPDs by providing the ionospheric uplift favorable for perturbations at the bottom side F-region to develop into EPDs.

Data Availability Statement

The Level 1C data used in this research are available at the GOLD Science Data Center (http://gold.cs.ucf.edu/search/). The Level 1b data from the Swarm mission are accessible via the website (https://earth.esa.int/swarm). Kp is provided by GFZ Potsdam (https://www.gfz-potsdam.de/en/kp-index/), and F10.7 by the Dominion Radio Astrophysical Observatory and Natural Resources Canada (https://www.spaceweather.gc.ca/solarflux/sx-en.php).

Acknowledgments
The authors thank Hermann Lühr for fruitful discussions. This study was supported by the German Research Foundation (DFG) through the Special Priority Programme 1788 "Dynamic Earth." SLE was supported by NASA contract 80GSFC18C0061. The authors acknowledge the support from the International Space Science Institute (ISSI) through the International Team "An Exploration of the Valley Region in the Low Latitude Ionosphere: Response to Forcing from Below and Above and Relevance to Space Weather." Open Access funding enabled and organized by ProjektDEAL. WOA Institution: N/A Blended DEAL: ProjektDEAL.

References

Alken, P., Maus, S., Chulliat, A., Vigneron, P., Sirol, O., & Hulot, G. (2015). Swarm equatorial electric field chain: First results. *Geophysical Research Letters*, *42*, 673–680. https://doi.org/10.1002/2014GL062658

Anderson, D., Araujo-Pradere, E., & Scherliess, L. (2009). Comparing daytime, equatorial E×B drift velocities and TOPEX/TEC observations associated with the 4-cell, non-migrating tidal structure. *Annals of Geophysics*, *27*(7), 2861–2867.

Appleton, E. V. (1946). Two anomalies in the ionosphere. *Nature*, *157*(3995), 691–691.

Basu, S., Kudeki, E., Basu, S., Valladares, C., Weber, E., Zengingonul, H., et al. (1996). Scintillations, plasma drifts, and neutral winds in the equatorial ionosphere after sunset. *Journal of Geophysical Research*, *101*(A12), 26795–26809.

Bruinsma, S. L., & Forbes, J. M. (2008). Medium- to large-scale density variability as observed by CHAMP. *Space Weather*, *6*, S08002. doi: 10.1029/2008SW000411

Chartier, A. T., Mitchell, C. N., & Miller, E. S. (2018). Annual occurrence rates of ionospheric polar cap patches observed using Swarm. *Journal of Geophysical Research: Space Physics*, *123*, 2327–2335. https://doi.org/10.1002/2017JA024811

Duncan, R. (1960). The equatorial F-region of the ionosphere. *Journal of Atmospheric and Terrestrial Physics*, *18*(2–3), 89–100.

Eastes, R., McClintock, W., Burns, A., Anderson, D., Andersson, L., Aryal, S., et al. (2020). Initial observations by the GOLD mission. *Journal of Geophysical Research: Space Physics*, *125*, e2020JA027823. https://doi.org/10.1029/2020JA027823

Eastes, R., Solomon, S., Daniell, R., Anderson, D., Burns, A., England, S., et al. (2019). Global-scale observations of the equatorial ionization anomaly. *Geophysical Research Letters*, *46*, 9318–9326. https://doi.org/10.1029/2019GL084199

England, S., Immel, T., Sagawa, E., Henderson, S., Hagan, M., Mende, S., et al. (2006). Effect of atmospheric tides on the morphology of the quiet time, postsunset equatorial ionospheric anomaly. *Journal of Geophysical Research*, *111*, A10S19. https://doi.org/10.1029/2006JA011795

Fejer, B. G., De Paula, E., Gonzalez, S., & Woodman, R. (1991). Average vertical and zonal F region plasma drifts over Jicamarca. *Journal of Geophysical Research*, *96*(A8), 13901–13906.

Fejer, B. G., Scherliess, L., & De Paula, E. (1999). Effects of the vertical plasma drift velocity on the generation and evolution of equatorial spread F. *Journal of Geophysical Research*, *104*(A9), 19859–19869.

Forbes, J., Marcos, F., & Kamalabadi, F. (1995). Wave structures in lower thermosphere density from satellite electrostatic triaxial accelerometer measurements. *Journal of Geophysical Research*, *100*(A8), 14693–14701.

Forbes, J., Zhang, X., Palo, S., Russell, J., Mertens, C., & Mlynczak, M. (2008). Tidal variability in the ionospheric dynamo region. *Journal of Geophysical Research*, *113*, A20310. https://doi.org/10.1029/2007JA012737

Gentile, L. C., Burke, W. J., & Rich, F. J. (2006). A global climatology for equatorial plasma bubbles in the topside ionosphere. *Annales Geophysicae*, 24(1), 163–172. https://doi.org/10.5194/angeo-24-163-2006

Guo, B., Xu, J., Sun, L., Lin, Y., & Yuan, W. (2020). The seasonal and longitudinal variations of nighttime OI 135.6 nm emission at equatorial ionization anomaly crests observed by the DMSP/SSUSI. *Journal of Geophysical Research: Space Physics*, *125*, e2019JA027764. https://doi.org/10.1029/2019JA027764

Hanson, W. (1969). Radiative recombination of atomic oxygen ions in the nighttime F region. *Journal of Geophysical Research*, *74*(14), 3720–3722.

Heelis, R. (2004). Electrodynamics in the low and middle latitude ionosphere: A tutorial. *Journal of Atmospheric and Solar-Terrestrial Physics*, *66*(10), 825–838.

Hoffmann, L., Xue, X., & Alexander, M. (2013). A global view of stratospheric gravity wave hotspots located with Atmospheric Infrared Sounder observations. *Journal of Geophysical Research: Atmospheres*, *118*, 416–434. https://doi.org/10.1029/2012JD018658

Huang, C.-S., & Hairston, M. R. (2015). The postsunset vertical plasma drift and its effects on the generation of equatorial plasma bubbles observed by the C/NOFS satellite. *Journal of Geophysical Research: Space Physics*, *120*, 2263–2275. https://doi.org/10.1002/2014JA020735

Hysell, D. (2000). An overview and synthesis of plasma irregularities in equatorial spread F. *Journal of Atmospheric and Solar-Terrestrial Physics*, *62*(12), 1037–1056.

Hysell, D., & Burcham, J. (2002). Long term studies of equatorial spread F using the JULIA radar at Jicamarca. *Journal of Atmospheric and Solar-Terrestrial Physics*, *64*(12–14), 1531–1543.

Hysell, D., & Kudeki, E. (2004). Collisional shear instability in the equatorial F region ionosphere. *Journal of Geophysical Research*, *109*, A11301. https://doi.org/10.1029/2004JA010636

Immel, T., Sagawa, E., England, S., Henderson, S., Hagan, M., Mende, S., et al. (2006). Control of equatorial ionospheric morphology by atmospheric tides. *Geophysical Research Letters*, *33*, L15108. https://doi.org/10.1029/2006GL026161

Kelley, M., Ilma, R., & Crowley, G. (2009). On the origin of pre-reversal enhancement of the zonal equatorial electric field. *Annals of Geophysics*, *27*(5), 2053–2056.

Kelley, M., Makela, J. J., Paxton, L. J., Kamalabadi, F., Comberiate, J. M., & Kil, H. (2003). The first coordinated ground-and space-based optical observations of equatorial plasma bubbles. *Geophysical Research Letters*, *30*(14), 1766. https://doi.org/10.1029/2003GL017301

Kil, H., Heelis, R. A., Paxton, L. J., & Oh, S.-J. (2009). Formation of a plasma depletion shell in the equatorial ionosphere. *Journal of Geophysical Research*, *114*, A11302. https://doi.org/10.1029/2009JA014369

Liu, H., Bardeen, C. G., Foster, B. T., Lauritzen, P., Liu, J., & Lu, G. (2018). Development and validation of the Whole Atmosphere Community Climate Model with thermosphere and ionosphere extension (WACCM-X 2.0). *Journal of Advances in Modeling Earth Systems*, *10*(2), 381–402.

Liu, H., Yamamoto, M., & Lühr, H. (2009). Wave-4 pattern of the equatorial mass density anomaly: A thermospheric signature of tropical deep convection. *Geophysical Research Letters*, *36*, L18104. https://doi.org/10.1029/2009GL039865

Makela, J., Vadas, S., Muryanto, R., Duly, T., & Crowley, G. (2010). Periodic spacing between consecutive equatorial plasma bubbles. *Geophysical Research Letters*, *37*, L14103. https://doi.org/10.1029/2010GL043968

Mayr, H., Harris, I., Herrero, F., Spencer, N., Varosi, F., & Pesnell, W. (1990). Thermospheric gravity waves: Observations and interpretation using the transfer function model (TFM). *Space Science Reviews*, *54*(3–4), 297–375.

Park, J., Yamazaki, Y., & Lühr, H. (2020). Latitude dependence of Interhemispheric Field-Aligned Currents (IHFACs) as observed by the Swarm constellation. *Journal of Geophysical Research: Space Physics*, *125*, e2019JA027694. https://doi.org/10.1029/2019JA027694

Richmond, A., Fang, T.-W., & Maute, A. (2015). Electrodynamics of the equatorial evening ionosphere: 1. Importance of winds in different regions. *Journal of Geophysical Research: Space Physics*, *120*, 2118–2132. https://doi.org/10.1002/2014JA020934

Rodríguez-Zuluaga, J., Stolle, C., Yamazaki, Y., Lühr, H., Park, J., Scherliess, L., & Chau, J. L. (2019). On the balance between plasma and magnetic pressure across equatorial plasma depletions. *Journal of Geophysical Research: Space Physics*, *124*, 5936–5944. https://doi.org/10.1029/2019JA026700

Singh, S., Johnson, F., & Power, R. (1997). Gravity wave seeding of equatorial plasma bubbles. *Journal of Geophysical Research*, *102*(A4), 7399–7410.

Spiga, A., Teitelbaum, H., & Zeitlin, V. (2008). Identification of the sources of inertia-gravity waves in the Andes cordillera region. *Annals of Geophysics*, *26*(9), 2551–2568.

Stolle, C., Lühr, H., & Fejer, B. G. (2008). Relation between the occurrence rate of ESF and the equatorial vertical plasma drift velocity at sunset derived from global observations. *Annales Geophysicae*, *26*, 3979–3988.

Su, S.-Y., Chao, C., & Liu, C. (2008). On monthly/seasonal/longitudinal variations of equatorial irregularity occurrences and their relationship with the postsunset vertical drift velocities. *Journal of Geophysical Research*, *113*, A05307. https://doi.org/10.1029/2007JA012809

Thampi, S. V., Yamamoto, M., Tsunoda, R. T., Otsuka, Y., Tsugawa, T., Uemoto, J., & Ishii, M. (2009). First observations of large-scale wave structure and equatorial spread F using CERTO radio beacon on the C/NOFS satellite. *Geophysical Research Letters*, *36*, L18111. https://doi.org/10.1029/2009GL039887

Tsunoda, R. T., Saito, S., & Nguyen, T. T. (2018). Post-sunset rise of equatorial F layeror upwelling growth? *Progress in Earth and Planetary Science*, *5*(1), 1–28.

Tsunoda, R. T., Yamamoto, M., Tsugawa, T., Hoang, T. L., Tulasi Ram, S., Thampi, S. V., et al. (2011). On seeding, large-scale wave structure, equatorial spread F, and scintillations over Vietnam. *Geophysical Research Letters*, *38*, L20102. https://doi.org/10.1029/2011GL049173

Vadas, S. L., & Liu, H.-L. (2009). Generation of large-scale gravity waves and neutral winds in the thermosphere from the dissipation of convectively generated gravity waves. *Journal of Geophysical Research*, *114*, A10310. https://doi.org/10.1029/2009JA014108

Xiong, C., Stolle, C., & Lühr, H. (2016). The Swarm satellite loss of GPS signal and its relation to ionospheric plasma irregularities. *Space Weather*, *14*, 563–577.